JOURNAL OF VIROLOGY, Nov. 2010, p. 11359–11373 Vol. 84, No. 21
0022-538X/10/$12.00 doi:10.1128/JVI.00804-10

Toll-Like Receptor 4-Mediated Activation of p38 Mitogen-Activated Protein Kinase Is a Determinant of Respiratory Virus Entry and Tropism[▽]

David Marchant, Gurpreet K. Singhera, Soraya Utokaparch, Tillie L. Hackett, John H. Boyd, Zongshu Luo, Xiaoning Si, Delbert R. Dorscheid, Bruce M. McManus,* and Richard G. Hegele*

UBC James Hogg Research Centre, Providence Heart + Lung Institute, Department of Pathology and Laboratory Medicine, University of British Columbia, Room 166, Burrard Building, St. Paul's Hospital, 1081 Burrard Street, Vancouver, British Columbia, Canada V6Z 1Y6

Received 15 April 2010/Accepted 28 July 2010

Respiratory viruses exert a heavy toll of morbidity and mortality worldwide. Despite this burden there are few specific treatments available for respiratory virus infections. Since many viruses utilize host cell enzymatic machinery such as protein kinases for replication, we determined whether pharmacological inhibition of kinases could, in principle, be used as a broad antiviral strategy for common human respiratory virus infections. A panel of green fluorescent protein (GFP)-expressing recombinant respiratory viruses, including an isolate of H1N1 influenza virus (H1N1/Weiss/43), was used to represent a broad range of virus families responsible for common respiratory infections (*Adenoviridae*, *Paramyxoviridae*, *Picornaviridae*, and *Orthomyxoviridae*). Kinase inhibitors were screened in a high-throughput assay that detected virus infection in human airway epithelial cells (1HAEo-) using a fluorescent plate reader. Inhibition of p38 mitogen-activated protein kinase (MAPK) signaling was able to significantly inhibit replication by all viruses tested. Therefore, the pathways involved in virus-mediated p38 and extracellular signal-regulated kinase (ERK) MAPK activation were investigated using bronchial epithelial cells and primary fibroblasts derived from MyD88 knockout mouse lungs. Influenza virus, which activated p38 MAPK to approximately 10-fold-greater levels than did respiratory syncytial virus (RSV) in 1HAEo- cells, was internalized about 8-fold faster and more completely than RSV. We show for the first time that p38 MAPK is a determinant of virus infection that is dependent upon MyD88 expression and Toll-like receptor 4 (TLR4) ligation. Imaging of virus-TLR4 interactions showed significant clustering of TLR4 at the site of virus-cell interaction, triggering phosphorylation of downstream targets of p38 MAPK, suggesting the need for a signaling receptor to activate virus internalization.

Respiratory virus infections cause considerable morbidity and mortality worldwide; it was recently reported that hospitalizations due to respiratory syncytial virus (RSV) exceed 2 million per year in the Unites States alone (16). An H1N1 swine influenza pandemic took place during the 2009-2010 winter season (14), and there is the lingering threat of an H5N1 avian influenza pandemic, with mortality due to direct bird-to-human H5N1 infection in hospitalized patients between 30 and 100% (3). The severe acute respiratory syndrome (SARS)-associated coronavirus, isolated in 2003, resulted in devastating respiratory tract infections with few treatment options (40). For most common respiratory viruses, treatment is symptomatic, and for pathogens such as influenza viruses for which specific treatments are available, oseltamivir (Tamiflu)- and amantidine-resistant strains are emerging and being transmitted globally (33).

All functions within a cell are triggered and regulated by cell signaling cues. Since viruses are obligate intracellular parasites, they rely upon cell signaling to regulate all processes within the cell that drive virus replication. In this study we investigated the effects of kinase inhibitors as a therapeutic strategy and to investigate the roles played by some kinases during virus replication. The extracellular signal-regulated kinase (ERK) and p38 mitogen-activated protein kinases (MAPKs) have been shown by us and others to play important roles during virus replication *in vitro* (19, 20, 26, 30, 42), and we have recently reported that inhibition of p38 MAPK activation is an effective and novel antiviral strategy *in vivo* (29). The significance of p38 MAPK activity *in vivo* is such that inadvertent and coincident activation of this kinase by some pharmaceutical agents enhances virus replication (29). Antiviral strategies may exist whereby inhibition of host cell kinases may stem the spread and replication of numerous different viral species. Such broad antiviral strategies would permit administration of kinase inhibitors to patients suspected of having respiratory viral infection, and to health care workers or inhabitants within the locale of a viral outbreak, prior to the availability of results from laboratory diagnostic testing.

The activation of p38 MAPK by pattern recognition receptors (PRRs) has been studied in the context of the antiviral immune response (reviewed in reference 22). We report here

* Corresponding author. Mailing address for Bruce M. McManus: UBC James Hogg Research Centre, Providence Heart + Lung Institute, Department of Pathology and Laboratory Medicine, University of British Columbia, Room 166, Burrard Building, St. Paul's Hospital, 1081 Burrard Street, Vancouver, British Columbia, Canada V6Z 1Y6. Phone: (604) 806-8586. Fax: (604) 806-9274. E-mail: bruce.mcmanus@hli.ubc.ca. Mailing address for Richard G. Hegele: Keenan Research Centre, Li Ka Shing Knowledge Institute, St. Michael's Hospital, Department of Laboratory Medicine and Pathobiology, University of Toronto, 1 King's College Circle, Toronto, Ontario, Canada M5S 1A8. Phone: (416) 978-2557. Fax: (416) 978-7361. E-mail: richard.hegele@utoronto.ca.

▽ Published ahead of print on 11 August 2010.

that viruses usurp these responses for the benefit of virus replication through activation of p38 MAPK, mediated by a PRR (Toll-like receptor 4 [TLR4]) and MyD88, providing the basis for a broad-spectrum antiviral.

MATERIALS AND METHODS

Viruses, cells, and inhibitors. Coxsackievirus B3 (CVB3)-green fluorescent protein (GFP), a molecular clone of CVB3 Woodruff (pH 3; GenBank accession no. U57056) containing an enhanced GFP (eGFP) expression cassette (CVB3-GFP) described previously (12, 44), was used in this study (provided by Ralph Feuer and J. Lindsay Whitton [The Scripps Institute, La Jolla, CA]). Influenza virus A/Weiss/43 (H1N1) (VR96) was obtained from the American Type Culture Collection (ATCC; Manassas, VA), and stocks were produced in HeLa cells in serum-free Dulbecco modified Eagle medium (DMEM) containing 10 μg/ml trypsin. For experiments, 1 vial of influenza virus was treated at 37°C in the presence of serum-free 10-μg/ml trypsin for 30 min prior to dilution and addition to cells. RSV-A2-GFP was provided by Mark Peeples (Department of Pediatrics, The Ohio State University, Children's Research Institute, Columbus, OH) (46, 49), and human parainfluenza virus type 3 (hPIV3)-GFP was provided by Peter Collins (National Institutes of Health, Bethesda, MD) (45, 48). Human adenovirus (AdV) 5 was obtained from ATCC (catalog no. VR-1516). AdV-GFP (adenovirus 5-derived delta E1 and E3 vector with GFP expression driven from a cytomegalovirus [CMV] promoter) was purchased from Vector Biolabs (Philadelphia, PA). All viruses except adenovirus E-deleted vector were produced in HeLa cells. Adenovirus vector stocks were produced in HEK 293 cells. In all experiments, infections were conducted in parallel with uninfected control-conditioned medium from HeLa cells to control for possible activation of cells by cell-conditioned medium.

Immortalized epithelial cell lines used were 1HAEo- (bronchial epithelial), A549 (alveolar epithelial), and HeLa (cervical carcinoma). These were cultured in DMEM-10% fetal bovine serum (FBS) and obtained from ATCC, except for 1HAEo- cells, which have been described previously (6).

Isolation of primary fibroblasts. All animals were treated humanely and in accordance with the regulations of the UBC Animal Care Committee and standards of the Canadian Council on Animal Care. Pulmonary fibroblasts were isolated from MyD88 knockout (KO) and wild-type (WT) C57 background control mouse lungs. Briefly, lungs were removed from mice that were first anesthetized by isofluorane and then euthanized by cervical dislocation. Lungs were minced briefly and placed into the appropriately sized tissue culture tray. Lung pieces were dried for approximately 5 min and overlaid with DMEM, 10% FBS, and penicillin-streptomycin. Lungs were removed on the following day, and cells were replated 1 week later.

Kinase inhibitors and chemicals. Inhibitors purchased from Tocris Pharmaceuticals (Ellisville, MO) were used at the final concentrations indicated (target kinase is in parentheses): API-2 (Akt/protein kinase B [PKB]), 1 μM; BAY11-7085 (NF-κB), 10 μM; LY294002 (phosphatidylinositol 3-kinase [PI3K]), 25 μM; MG132 (proteasome), 10 μM; PP2 (Src family kinases), 5 μM; SB203580 (p38 MAPK), 5 μM; SB216763 (glycogen synthase kinase 3β [GSK3β]), 10 μM; SP600125 (Jun N-terminal protein kinase [JNK]), 20 μM; U0126 (MEK1/2), 20 μM. Anisomycin was purchased from Sigma-Aldrich (St. Louis, MO) and used at a concentration of 10 μM.

Correlation of PFU with GFP IU/ml. Infected cultures of each of the recombinant viruses used were subject to plaque assay in parallel to flow cytometry of GFP expression of infected cultures, at least once. Infectious units per ml (influenza virus staining) or GFP-positive (GFP^+) cells per ml were calculated by multiplying the proportion of Alexa 594 (influenza virus)- or GFP-positive cells by the total number of cells in the well, resulting in the total number of infected cells. This value was divided by the dilution factor and the volume of inoculum in ml, which is the number of GFP^+ cells per ml (recombinant GFP viruses) or infectious units per ml (IU/ml; influenza virus).

Antibodies. Antiadenovirus monoclonal antibody (MAb) 8052 from Chemicon International (clone 20/11; Millipore, Billerica, MA) detects the hexon protein of most adenoviruses. Anti-VP1 of CVB3 was purchased from Novocastra (antienterovirus VP1 clone D5/8; Newcastle, United Kingdom); goat anti-influenza H1N1 virus catalog no. 18-783-77828-1 was purchased from GenWay Biotech (San Diego, CA); anti-RSV3 mouse monoclonal glycoprotein F, protein P, and protein N antibodies were purchased from Novocastra. Goat anti-RSV (all antigens) polyclonal antibody was purchased from Biodesign International (Saco, ME; catalog no. B65860G). Parainfluenza virus type 3 was detected by Western blotting using goat anti-parainfluenza virus 2 and 3 polyclonal sera from Biodesign International (catalog no. B65130). Anti-Toll-like receptor 4 goat polyclonal IgG and monoclonal humanized IgA antibodies were purchased from AbCam (ab53629) and Invivogen (catalog no. maba2-htlr4), respectively. The RSV nucleoprotein (N) was detected using a mouse monoclonal antibody (ab10016) that detects only mature virion N protein.

Determination of infectivity via flow cytometry. Influenza virus infection was measured by antibody staining followed by flow cytometry. Briefly, cells were detached and fixed in 5 mM EDTA and 3% formalin, respectively. Cells underwent centrifugation (500 × *g*, 5 min) and were reconstituted in phosphate-buffered saline (PBS), 0.3% Triton X-100, and 1% bovine serum albumin (BSA) for 10 min at room temperature (RT). Goat anti-influenza was added at a 1/100 dilution for 30 min at RT in 0.3% Triton X-100, 1% BSA, and PBS. Cells were washed by 3 consecutive centrifugation (500 × *g*, 3 min) and PBS washing steps with 5 min between each wash. Secondary Alexa 594 donkey anti-goat antibody was added at a 1/200 dilution in 0.3% Triton X-100 in PBS for 30 min at RT. Cells were washed 3 times and enumerated with a Beckman Coulter Epics XL-MCS flow cytometer.

Determination of viral genome copy number in cell-free virus via quantitative reverse transcription-PCR (RT-PCR). Virus RNA or adenovirus DNA was extracted from cell-free virus aliquots using the viral RNA minikit or DNA blood and tissue minikit, respectively (Qiagen, Mississauga, ON, Canada). Sequences for the primers and probes for each respiratory virus were chosen using Primer Express software (Applied Biosystems, Foster City, CA) following recommended criteria. Synthetic standards were produced for each virus to allow absolute quantification of cDNA from the virus aliquots. The standards were comprised of pGEM4Z (Promega, Madison, WI) incorporating the target amplicon of each virus. A restriction site integrated within the amplicon allowed for the detection of any cross-contamination between the virus aliquot specimen and the synthetic one. Briefly, RNA with priming sites and amplification attributes identical to those of the real viral target was created from the synthetic standard. Twenty micrograms of plasmid DNA was linearized using 40 U of XbaI for 2 h at 37°C and then heated at 65°C for 15 min to inactivate the XbaI. Two micrograms of digested plasmid was *in vitro* transcribed using a MEGAshortscript kit (Ambion, Austin, TX). Transcription buffer, deoxynucleoside triphosphates (dNTPs), plasmid, and enzyme mix were combined to a final volume of 20 μl and incubated for 2 h. RNase-free DNase I was added to the reaction mixture and allowed to incubate at 37°C for an additional 15 min to remove template DNA. To recover the transcript, RNA was purified by ammonium acetate precipitation. The RNA pellet was then resuspended in 100 μl of RNase- and DNase-free water. The cDNA produced from the *in vitro*-transcribed transcripts was serially diluted from 10^8 to 10^1 copy numbers, aliquoted, and stored along with the specimen cDNA at −80°C until use. Quantitative PCR assays were performed on an ABI 7900HT (Applied Biosystems, Foster City, CA) machine in triplicate.

Kinase inhibitor screen of GFP-virus-infected cells. HeLa, 1HAEo-, or A549 cells were seeded at confluence in 96-well optical-bottom plates. Kinase inhibitors were added 30 min prior to infection, and AdV-GFP, RSV-GFP, and hPIV3-GFP infection mixtures at multiplicities of infection (MOI) of 1 and 10 were fixed in methanol-acetone (3:1, vol/vol) 24 h postinfection. CVB3 infection mixtures were harvested 8 to 10 h postinfection. GFP fluorescence was detected and quantified by a Tecan GENios fluorescence plate reader (excitation [Ex], 485/emission [Em], 535; gain, 60; MTX Lab Systems). Infections were then treated with Hoechst 33342 (1/10,000 for 10 min) to stain nuclei, and fluorescence was detected (Ex, 360/Em, 465; gain, 60) as a cell input control.

The activity of kinase inhibitors upon influenza virus infection was detected by antibody staining of influenza virus protein at 16 h postinfection and enumeration by flow cytometry. Kinase inhibitors were added 30 min prior to infection, and influenza virus-infected cells were detached with 5 mM EDTA and fixed with 3.7% formalin-PBS for 10 min. Cells were stained using polyclonal anti-influenza virus sera as outlined above.

Determination of cell viability by 3-(4,5-dimethylthiazol-2-yl)-5-(3-carboxymethoxyphenyl)-2-(4-sulfophenyl)-2H-tetrazolim assay. Cell viability was determined with the Promega MTS assay kit (Madison, WI), per the manufacturer's instructions.

Determination of MAPK phosphorylation by phospho-ELISA and Western blot assay. Cells were seeded into 12- or 24-well trays and infected with virus or cell-conditioned medium in 10% FBS-DMEM. Cell lysates were harvested using protein lysis buffer (10 mM HEPES [pH 7.4], 50 mM $Na_4P_2O_7$, 50 mM NaF, 50 mM NaCl, 5 mM EDTA, 5 mM EGTA, 1 mM Na_3VO_4, 0.5% Triton X-100, 10 μg/ml leupeptin, and 1 mM phenylmethylsulfonyl fluoride). Ten micrograms of sample was loaded per well of each enzyme-linked immunosorbent assay (ELISA) mixture. ERK, JNK, ATF2, and p38 MAPK phosphorylation was determined using ELISA kits purchased from Biosource (Invitrogen, Carlsbad, CA). Samples were assayed per the manufacturer's instructions. To better visualize increases in MAPK phosphorylation in Fig. 1a to d, the basal levels of

MAPK activation (conditioned medium) were subtracted from the values obtained from the virus-infected cells at each time point.

Western blot assay. Alternatively, lysates were subjected to Western blotting, whereby cells were harvested in protein lysis buffer, as described above. Postnuclear supernatant was harvested by centrifugation at 14,000 × *g* for 10 min at 4°C, boiled and resolved on a 12% polyacrylamide gel at 120 V for 1 h, and transferred to a nitrocellulose membrane. Lysates were probed for RSV, CVB3, p42/p44 total ERK MAPK, MyD88, and total and phospho-p38 MAPK.

Neutralization of Toll-like receptor 4 signaling with a neutralizing antibody. 1HAEo- and HeLa cells were treated with a dilution series of rabbit IgG control (ab46540) and rabbit polyclonal anti-human TLR4 antibody from AbCam (ab13556; Cambridge, MA), in serum-free DMEM. Cells were infected with a dilution series of RSV-A2 and influenza virus H1N1/Weiss/43 with 1 h of preincubation with anti-TLR4 or control antibodies. Infected cells were enumerated by flow cytometry the following day, and lysates were harvested for Western blotting in parallel to monitor successful inhibition of phospho-p38 MAPK or phospho-ATF-2 (see "Western blot assay" above). Influenza virus-infected cells were enumerated by flow cytometry after antibody staining (described under "Determination of infectivity via flow cytometry").

Detection of virus particles and host cell proteins using immunofluorescence confocal microscopy. Immunofluorescence of virus during cell entry has been described previously (30). Virus (MOI, 3 to 5) was added to cells on ice for 1 h, cells were washed once with PBS, and infection proceeded in a 37°C incubator until the indicated time points. Cells were fixed by addition of room temperature 3:1 (vol/vol) methanol-acetone for 2 min and blocked with 1% BSA-PBS or blocked and permeabilized with 0.3% Triton X-100, 1% BSA, and PBS (PERM buffer) for 10 min at room temperature. Primary antibodies were added at a 1/100 dilution at 4°C overnight in PERM buffer. Rabbit anti-phospho-ATF2 (catalog no. 9221; Cell Signaling technologies, Danvers, MA) and goat anti-TLR4 (ab53629; AbCam, Cambridge, MA) were stained with goat anti-rabbit or donkey anti-goat secondary antibodies conjugated to Alexa 488 or 594, at a dilution of 1/400 in PERM buffer. The goat anti-rabbit secondary antibody was added after the donkey anti-goat antibody, with an additional wash step, to prevent secondary antibody cross-reactivity, in the experiments that required mouse (RSV3 MAbs), goat (TLR4), and rabbit (phospho-ATF2) antibody detection. Virus was stained with monoclonal anti-RSV (RSV3; a mix of 3 monoclonal RSV antibodies: glycoprotein F, protein P, and protein N [Novocastra]) and Alexa 405 or 488 secondary antibodies purchased from Invitrogen. Each step was followed with 3 washes in PBS of 5 min each. Nuclei were stained with DAPI (4′,6-diamidino-2-phenylindole) contained within the mounting medium, Vectashield (Vector Laboratories, Burlingame, CA). The non-PERM staining control assays were conducted as described above but in the absence of 0.3% Triton X-100.

Image acquisition, 3-dimensional modeling, and rendering. Immunofluorescence confocal microscopy was conducted using an AOBS Leica confocal TCS SP2 microscope (63×/numerical aperture [NA], 1.2) (Heidelberg, Germany). Lambda scans were performed throughout the experiments to confirm the specificity of Alexa Fluor dyes. Sequential scans prevented the detection of artifactual colocalization. The AOBS SP2 system allows for user-defined photo multiplier tube (PMT) filters of custom bandwidth, for specific and custom detection of each fluorophore by a separate PMT detector. Our purpose for this system was the exclusion of bleed-through of signal into the emission profile of fluorophores with longer wavelengths from fluorophores with emission at shorter wavelengths. Image stacks (100 to 150 × 512 × 512 pixels; 6-frame average) were collated using Improvision Volocity v5 software (Coventry, United Kingdom), with minor brightness and contrast adjustment (not greater than 20% of original values). Minor background noise filtering was conducted for all fluorescence confocal images using the fine noise filter in Volocity. Virus particles were counted automatically in a defined region of interest (ROI) at $t = 0$ min for RSV and influenza virus using the measurement function, detected by intensity greater than 30% and larger than 0.05 μm. The ROI was drawn around each DAPI-stained nucleus with an extra 1-μm buffer to isolate each individual cell for determination of the number of virus particles per cell.

Pearson's correlation. Pearson's correlation of image stacks was conducted to correlate overlap of image voxels (pixels in 3 dimensions) from 2 different channels using Volocity software (as described previously [29]). A value of +1 indicates complete voxel-to-voxel overlap of the voxels from 2 channels, throughout the image Z-stack. A value of 0 indicates random correlation of voxels from 2 different channels, and −1 indicates complete disparity of voxels from the 2 channels that have been compared.

Statistical methods. Statistical significance between two experimental groups was determined using Student's *t* test. Comparisons involving more than two experimental groups were conducted using analysis of variance (ANOVA) with Tukey's family comparison to determine statistical significance between the comparisons. A P value of <0.05 was considered to be significant.

RESULTS

Suppression of p38 MAPK activation with SB203580 inhibited infection by every virus in a screen of kinase inhibitors using 1HAEo- bronchial epithelial cells. Human airway epithelial cells (1HAEo-) were treated with pharmacological inhibitors to major host cell kinases for 30 min prior to infection, as we have previously described: JNK (SP600125) (42), ERK (U0126) (26, 30), and p38 (SB203580) (42) MAPKs; Src kinase (PP2) (47); PI3K (LY294002) (37); NF-κB (BAY11-7085) (8); Akt (API-2) (9, 10); and GSK3β (SB216763) (47). Plates were fixed, and GFP fluorescence produced by GFP-virus replication was detected by a fluorescence plate reader. Readouts were normalized to the no-treatment (dimethyl sulfoxide [DMSO]) control and by using Hoechst 33342 nuclear stain fluorescence. Figure 1 shows the magnitude of GFP fluorescence produced 8 to 10 h after infection with CVB3 (30) (Fig. 1a) and 24 h after infection with hPIV3-GFP (Fig. 1b), RSV-GFP (Fig. 1c), and AdV-GFP (Fig. 1d). Figure 1e shows the infectivity of H1N1 influenza virus in the presence of kinase inhibitors. These viruses represent four respiratory virus families (AdV; *Adenoviridae*, RSV/hPIV3; *Paramyxoviridae*, CVB3; *Picornaviridae* [respiratory transmission reviewed in reference 39], influenza A H1N1 virus; *Orthomyxoviridae*) and two subfamilies (RSV, subfamily *Pneumovirinae*, genus *Pneumovirus*; hPIV3, subfamily *Paramyxovirinae*, genus *Respirovirus*) within the *Paramyxoviridae* family.

The pharmacologic agents that inhibited replication of all viruses tested targeted p38 (SB203580) and ERK (U0126) MAPKs. There were 2.8-fold ($P = 0.04$), 3.6-fold ($P = 0.005$), 3.2-fold ($P = 0.002$), 1.7-fold ($P = 0.04$) and 9.4-fold ($P = 0.01$) decreases in fluorescence intensity of CVB3-GFP, hPIV3-GFP, RSV-GFP, AdV-GFP, and influenza H1N1 virus infections associated with SB203580 treatment compared to untreated controls, respectively (Fig. 1a to e). A549 (alveolar [type 1 pneumocyte] epithelial) cells and HeLa (cervical carcinoma) cells were also tested by this method with similar results: suppression of p38 using SB203580 consistently inhibited infection by all viruses tested (data not shown).

Cell viability curve of SB203580 compared to cisplatin after 24 h of treatment. Prior to further investigating a potential antiviral role for p38 inhibition, we tested the toxicity of SB203580 on the viability of 1HAEo- cells. We determined cell viability at 24 h in the presence of cisplatin or SB203580 as measured by MTS assay (Fig. 1f). As expected, cisplatin was cytotoxic in a dose-dependent manner, in which MTS absorbance at 500 nm decreased in a concentration-dependent manner. In contrast, SB203580 had little or no effect on MTS-related cell viability when administered in concentrations as high as 333 μM, suggesting that SB203580 did not inhibit virus replication via host cell death.

Virus-activated phosphorylation of p38 and ERK MAPKs is biphasic. We determined the activation profile of p38 and ERK MAPKs during virus infection to identify the points in the virus life cycle that were most susceptible to the p38 inhibitor SB203580. We added CVB3, hPIV3, RSV, and a laboratory-adapted strain of H1N1 influenza virus, at an RNA ge-

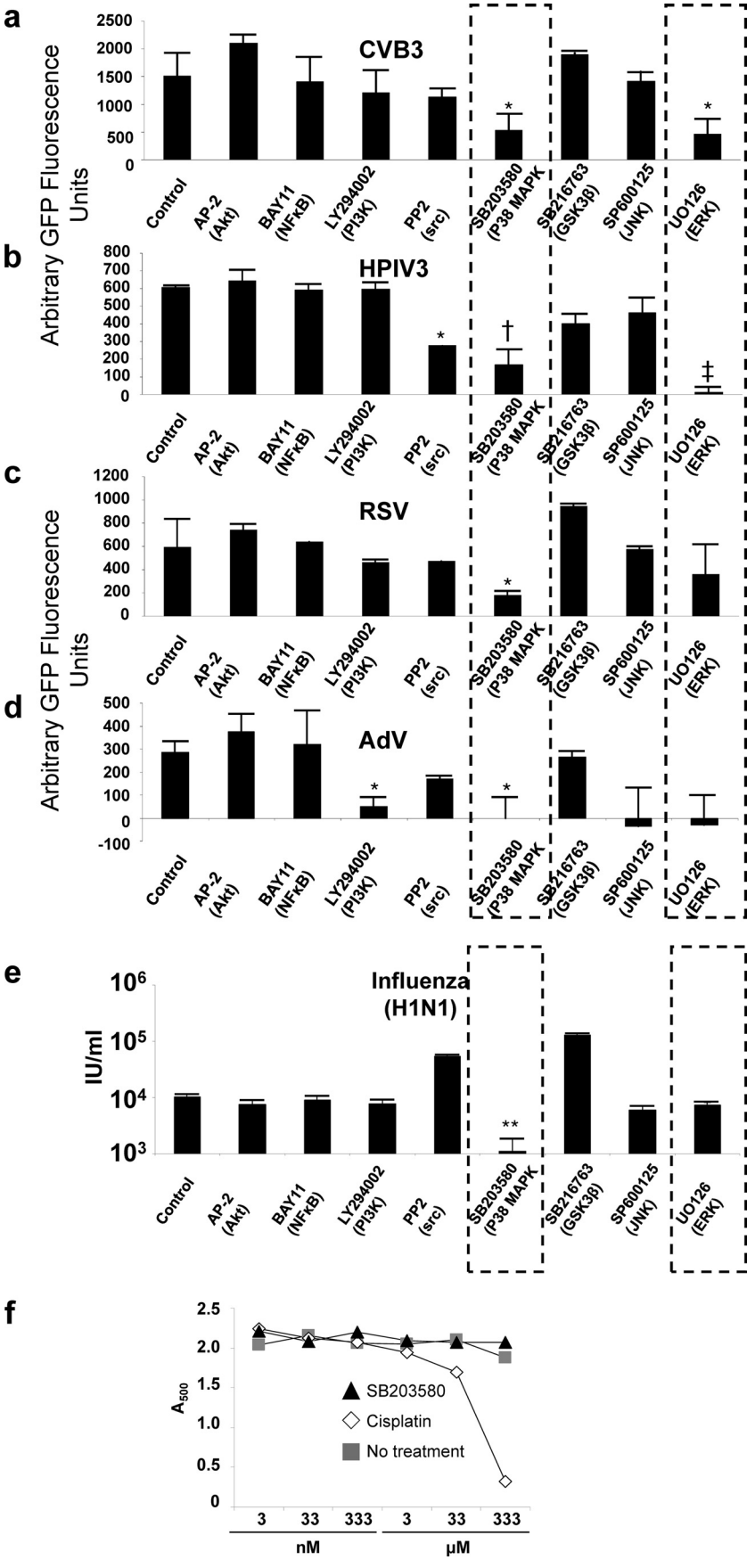
a
CVB3
b
HPIV3
c
RSV
d
AdV
Arbitrary GFP Fluorescence Units
e
Influenza (H1N1)
IU/ml
f
SB203580
Cisplatin
No treatment
A500
nM
μM
Control
AP-2 (Akt)
BAY11 (NFκB)
LY294002 (PI3K)
PP2 (src)
SB203580 (P38 MAPK)
SB216763 (GSK3β)
SP600125 (JNK)
UO126 (ERK)

nome copy number of 10 per cell, to 1HAEo- cells. Adenovirus was added at a DNA copy number of about 10 per cell. Genome copy numbers of virus stocks were determined by quantitative PCR against an in-house standard curve for each virus [see Materials and Methods, "Determination of viral genome copy number in cell-free virus via quantitative reverse transcription-PCR (RT-PCR)"] as a means of standardizing the virus particle input. A time course assay was conducted, and the phosphorylation states of ERK and p38 were determined by phospho-ELISA (Fig. 2a), as well as JNK (data not shown and reference 42). All viruses activated p38 MAPK 10 min postinfection, except for CVB3, which, in addition to cell-conditioned medium, was used as an internal control for p38 activation given that this virus activated p38 weakly or not at all during entry, 10 min postinfection (42). Human PIV3 ($P = 0.001$), RSV ($P = 7.9 \times 10^{-5}$), AdV ($P = 0.01$), and influenza virus ($P = 0.03$) activated p38 MAPK 10 min postinfection. At this time point influenza virus activated p38 to the highest level (3.1×10^2 U/ml) and AdV activated p38 to the lowest level (1.6×10^1 U/ml). In addition, influenza virus activated p38 MAPK to a 9.7-fold-higher level than did RSV (3.2×10^1 U/ml) at 10 min (Fig. 2a). As reported previously, CVB3 activated ERK 1 h postinfection and again at 8 h postinfection (27). Phosphorylation of ERK and p38 corresponded with the onset of virus protein production 8 h postinfection as determined by the detection of capsid protein VP1 (data not shown). Human PIV3 ($P = 0.03$), RSV ($P = 7.0 \times 10^{-4}$), and AdV ($P = 0.05$) activated p38 at 8 h postinfection. The activation of p38 and ERK MAPKs at 8 h postinfection was associated with the onset of virus protein production at approximately this time point, except for RSV, for which protein synthesis was not apparent until 16 h postinfection (data not shown).

We wanted to determine the point in the virus life cycle (Fig. 2b) at which p38 MAPK phosphorylation was a requirement of virus replication. Figure 2c shows how p38 inhibitor SB203580 inhibited RSV protein production at 8 h postinfection when added at 0.16 h (10 min) postinoculation, compared to the no-treatment control and the addition of SB203580 at 4 h postinoculation (i.e., after virus had successfully entered target cells). In contrast, CVB3 showed decreased VP1 production when SB203580 was added at both early (0.16 h) and later (4 h) time points postinfection. This difference is reflected in the different p38 MAPK activation profiles of RSV and CVB3 (Fig. 2a).

Early activation of p38 MAPK during virus entry is dependent upon MyD88. Influenza virus, hPIV3, RSV, and AdV produced identical profiles of p38 MAPK activation in 1HAEo- cells at 10 min postinfection (Fig. 2a). Therefore, we postulated that PRRs such as the Toll-like receptors (TLRs) may recognize high-mannose residues expressed on the surface of viruses (17, 21) or the virus surface glycoproteins that mediate virus entry into the host cell (15, 23, 38). As viruses interact with the surface of the cell, before or during entry receptor ligation, we reasoned that viruses might interact with PRRs expressed at the cell surface and initiate signaling and a response that affects virus uptake into the cell.

We isolated pulmonary fibroblasts from myeloid differentiation factor 88 (MyD88) KO mice. Myeloid differentiation factor 88 is a signaling adaptor that is required for the signal propagation of many of the Toll-like receptors (TLRs) (35). Therefore, determining the ERK and p38 MAPK activation profiles in MyD88 KO cells may implicate or rule out TLR involvement in MAPK activation 10 min post-virus infection. So we determined the expression of ERK MAPK, p38 MAPK, and MyD88 in MyD88 KO cells (Fig. 3a) compared to their expression in WT cells. As expected, there were equivalent amounts of ERK and p38 in WT and MyD88 KO cells, and MyD88 was absent from the KO cells.

We wanted to determine the ERK and p38 MAPK activation profiles in the WT and MyD88 KO cells during an 8-h infection time course. We postulated that activation of p38 and ERK may occur through a TLR pathway given the very early activation of p38 and ERK, 10 min postinfection (Fig. 2a). As postulated, we observed a lack of p38 activation in murine MyD88 KO pulmonary fibroblasts upon virus entry, compared to the p38 MAPK activation that occurs in WT cells within 1 h of virus addition (Fig. 3b); however, there was apparent enhancement of ERK activation 10 min postinfection. The different activation profiles of p38 and ERK in MyD88 KO cells during virus entry are an indication of the different mechanisms/pathways of activation of these two MAPKs: in pulmonary fibroblasts p38 is apparently MyD88 dependent and ERK is MyD88 independent. Furthermore, we noted that p38 activation occurred in primary WT fibroblasts 10 to 15 min later than it did in the 1HAEo- cell line, explained by the inherent differences between primary cells and cell lines and fibroblasts and epithelial cells.

Figure 3c shows that there was significantly less virus infection of MyD88 KO cells than of WT cells. Adenovirus vector, influenza virus, and RSV infections were 14-, 2.3-, and 6.0-fold lower in MyD88 KO cells than in cells from the WT counterparts, respectively.

FIG. 1. The p38 and ERK MAPKs are principal kinases during host cell infection by a broad array of respiratory viruses. (a to d) Human airway epithelial (1HAEo-) cells were treated with kinase inhibitors for 1 h and infected with CVB3-eGFP (a), hPIV3-eGFP (b), RSV-eGFP (c), and AdV-eGFP (d), at MOI of 1 and 10, and GFP production as an indicator of virus infectivity was detected on a fluorescence plate reader on the following day. (e) Human airway epithelial (1HAEo-) cells were treated with kinase inhibitors for 1 h and infected with H1N1 influenza virus. Infectivity was determined by fluorescent antibody staining and flow cytometry on the following day: cells (1HAEo-) were treated with kinase inhibitors for 1 h and infected with influenza virus H1N1/Weiss/43 at an MOI of 0.01 to 1. Cells were harvested, fixed, and permeabilized 24 h later and stained for H1N1 influenza virus antigen with a polyclonal antibody followed by an Alexa 594 anti-goat secondary antibody, and infected cells were enumerated by flow cytometry. IU/ml, infectious units per ml. (f) Cisplatin but not SB203580 is cytotoxic to cells in a dose-dependent manner. 1HAEo- cells were treated with cisplatin and SB203580 and control DMSO in a dose titration (3 nM to 333 μM). Cell viability was measured by MTS assay at 24 h post-drug addition. The substrate MTT [3-(4,5-dimethylthiazol-2-yl)-2,5-diphenyltetrazolium bromide, a yellow tetrazole] is reduced to MTS [3-(4,5-dimethylthiazol-2-yl)-5-(3-carboxymethoxyphenyl)-2-(4-sulfophenyl)-2H-tetrazolium] by mitochondrial reductase in living cells. Loss of cell viability due to the treatment of cells with cisplatin is indicated by reduced absorbance at 33 and 333 μM, but there was no loss of cell viability with increasing doses of SB203580.

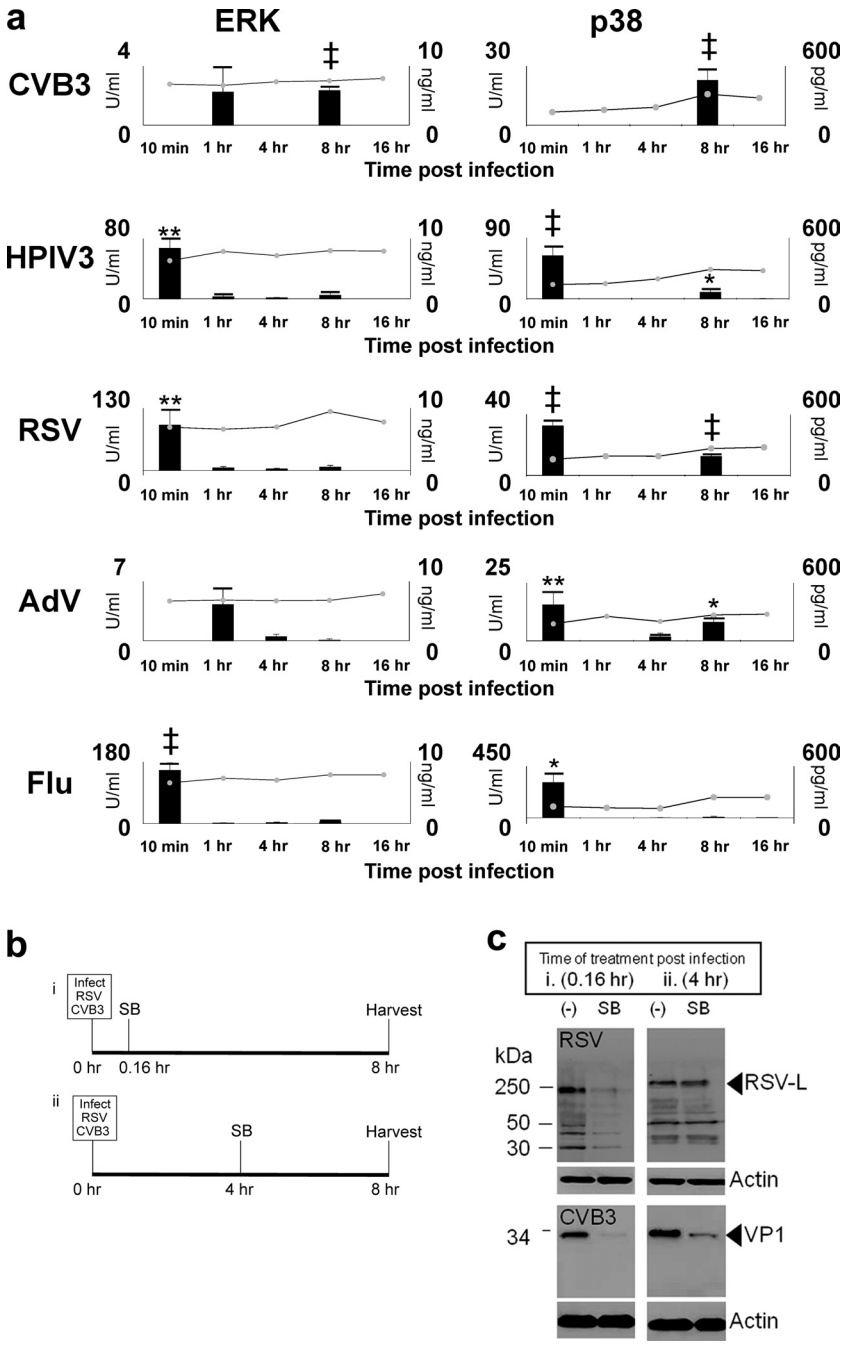

FIG. 2. The p38 and ERK MAPKs are activated at virus-host cell entry and late time points postinfection. (a) Cells (1HAEo-) were infected with viruses using 10 genome equivalents per cell as determined by qPCR of virus stocks (Materials and Methods), and cell lysates were harvested using cell lysis buffer at indicated time points. Phospho-ERK (bar graph) and total ERK (line chart) (left panels) and p38 MAPK activation (right panels) were detected using phospho-ELISA and total kinase ELISA kits. (b) Timeline of virus inoculation and SB203580 (SB) treatment for the pulse-chase experiment shown in panel c. (c) Cells were inoculated with virus and treated with SB as in panel b, and cell lysates were collected using cell lysis buffer. The Western blot shows that SB treatment (p38 MAPK inhibition) inhibited RSV protein production when added at 10 min post-virus inoculation but that SB inhibited CVB3 when it was added at both early (0.16 h [10 min]) and later (4 h) time points. Results are representative of at least 3 independent experiments.

Anisomycin is an antibiotic that activates p38 and JNK MAPKs (5, 18, 34). We wanted to determine whether p38 MAPK was a determinant of infection and tropism in target host cells. JNK was excluded since its inhibitor SP600125 did not affect viral replication (Fig. 1a to e), and the activation of JNK was particularly weak compared to the activation profiles of p38 and ERK MAPKs (data not shown). Therefore, we determined whether supplementary ectopic p38 activation could rescue virus infection in MyD88 KO cells, given that p38 was the MAPK not activated in these cells. We observed the

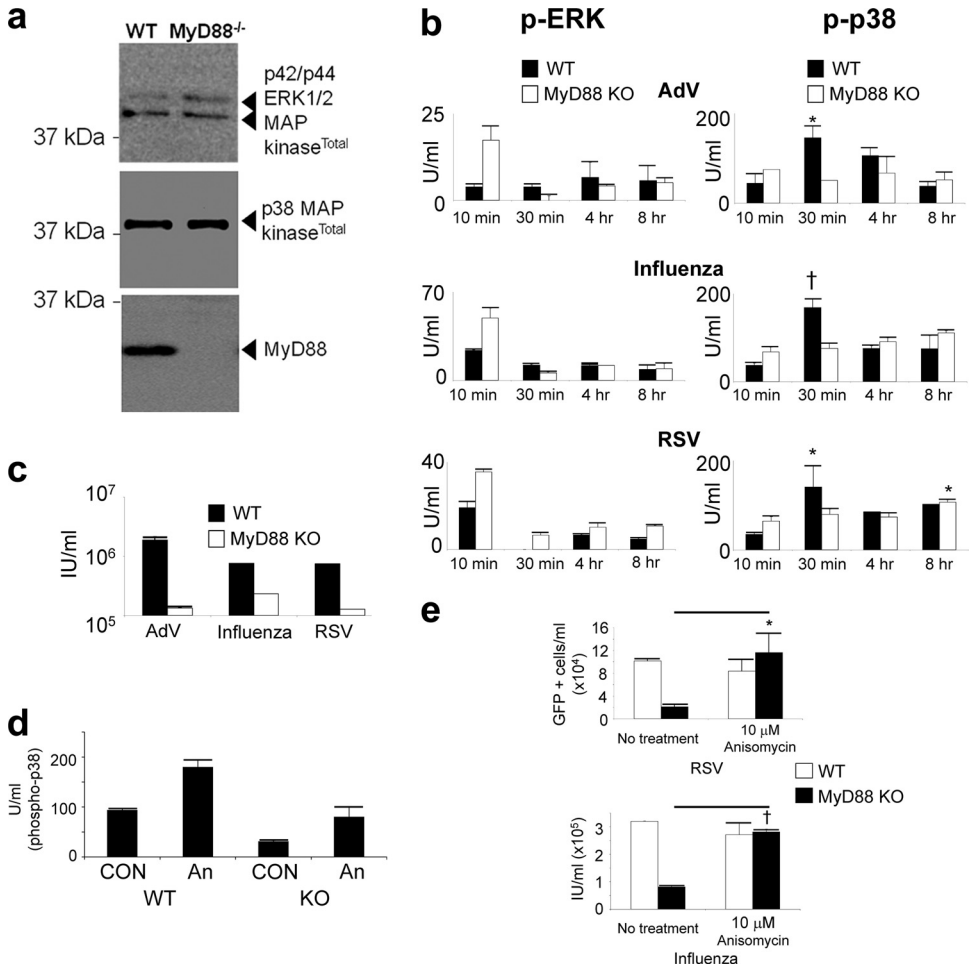

FIG. 3. Virus infection of MyD88 KO cells activates ERK but not p38 MAPK, resulting in less viral replication. (a) MyD88 KO cells express equivalent amounts of ERK and p38 MAPKs. Cell lysates were harvested, and p38 and ERK MAPKs and MyD88 were detected by Western blotting. (b) Equivalent numbers of MyD88 KO and WT C57 pulmonary fibroblasts were infected with 10 DNA genome copies/cell AdV and 10 RNA genome copies of influenza virus and RSV and harvested using cell lysis buffer at the indicated time points. Units/ml of phosphorylated p38 and ERK were determined by phospho-ELISA. Results are representative of 2 independent experiments. (c) Cells were infected as in panel b, but cells were harvested on the following day, fixed, and permeabilized, and the infectious units per ml (IU/ml) were determined 12 to 16 h later by flow cytometry for AdV-GFP and RSV-GFP by detection of peak fluorescence at 520 nm. Influenza virus titer was determined as in Fig. 1e by antibody staining and Alexa 594 fluorescence detection. Results show that MyD88 KO cells are less infectable with virus than are WT cells. Results are representative of 3 independent experiments. (d) ATF2 can be activated in MyD88 KO cells during virus entry in the presence of anisomycin. Wild-type and MyD88 KO cells were infected with RSV at an MOI of 1 with or without 10 μM anisomycin, and the level of phospho-p38 was detected by phospho-ELISA of cell lysates at 25 min postinfection. Error bars denote the standard deviation. CON, control; An, anisomycin. (e) Anisomycin treatment during virus entry recovers virus infection of MyD88 KO cells to WT levels. Cells were infected with RSV and influenza virus using MOI of 0.01 to 0.1 or infected and treated simultaneously with 10 μM anisomycin during virus entry and washed with fresh medium after 1 h, and infection was quantified by flow cytometry 12 to 16 h later. RSV infection was measured by detection of GFP fluorescence at 520 nm, and influenza virus infection was detected by primary and secondary Alexa 594 antibody staining followed by measurement of infectivity by flow cytometry, as in Fig. 1e. Results are representative of 3 independent experiments.

strongest profile of p38 activation at the 10-min entry time point, and so 10 μM anisomycin was added to culture with virus inoculum and washed out of culture after 1 h of virus incubation with the cells. We determined the effect of anisomycin treatment on p38 MAPK activation in RSV-infected WT and MyD88 KO fibroblasts after 30 min of anisomycin/RSV treatment, using p38 phospho-ELISA (Fig. 3d). Wild-type cells show activation of p38 within the first 30 min of infection that is 3.0-fold lower in KO cells (94 ± 26 U/ml in WT cells versus 31 ± 14 U/ml in KO cells). However, anisomycin treatment recovered virus-induced p38 activation in MyD88 KO cells (84 ± 16 U/ml), showing that p38 activation can be restored in KO cells by anisomycin treatment.

ATF2 phosphorylation is recovered in MyD88 KO cells using anisomycin. We measured ATF2 phosphorylation as a downstream marker of p38 MAPK activation (29).

We treated WT and MyD88 KO primary fibroblast cells with 10 μM anisomycin during inoculation with H1N1 influenza virus and RSV-A2, and infection was measured the following day (Materials and Methods). We wanted to determine whether rescue of p38 MAPK signaling in MyD88 KO cells could recover influenza virus and RSV-A2 infection in these

cells to WT levels. Influenza virus and RSV were chosen since they are enveloped viruses and activated p38 MAPK to the highest levels among the viruses studied (Fig. 2a). Influenza virus and RSV infections were recovered in the anisomycin-treated MyD88 KO cells to WT levels (Fig. 3e). Taken together, the results in Fig. 3 emphasize the importance of p38 MAPK activation via MyD88, in preference to ERK MAPK activation, to trigger virus entry and replication.

Imaging the signaling and entry of RSV and influenza virus in 1HAEo- airway bronchial epithelial cells. We imaged RSV and influenza virus during the entry phase of the virus life cycle to determine the effect of SB203580 on these 2 viruses during entry. We were also curious as to any potential differences between entry phases since p38 MAPK was activated to 10-fold-greater levels during influenza virus entry (310 ± 84 U/ml) than were seen at 10 min post-RSV infection (31 ± 34 U/ml [Fig. 2a]).

Activation of p38 MAPK signaling occurs at the site of virus-host cell contact. We wanted to determine the origin in the cell where virus activated p38 MAPK during entry, by visualizing the phosphorylation of p38 immediate downstream targets. Cells were treated with SB203580 or control (DMSO), and a time course of virus entry and phospho-ATF2 signaling was followed. Figure 4a shows a 40-min time course of RSV entry. We observed that phospho-ATF2, a downstream target of activated p38 MAPK, was phosphorylated above virus particles (10 min postinfection, YZ and XZ sections) or adjacent to the site of virus-cell interaction (10 min postinfection, XY section, and 25 min postinfection). At 40 min postwarming, under control conditions in Fig. 4b, we noted that RSV particles were located apically and in close perinuclear apposition. However, treatment with p38 MAPK inhibitor SB203580 resulted in virus particles located at the basal periphery of the target cells. Successful RSV replication is therefore associated with localization to apical perinuclear regions in the cell within 40 min of entry trafficking.

Activation of p38 MAPK was associated with virus trafficking to perinuclear regions and emergence of the RSV nucleoprotein during entry into the host cell. The close nuclear association of RSV virions after entry permitted quantitative analysis of internalized particle proximity to the nucleus (Fig. 4c) and correlation with successful virus entry. We used Pearson's correlation to determine the proximity of RSV to the nucleus during permeabilization control assays. The Pearson correlation ranges from +1 to −1, whereby a correlation of +1 indicates complete overlap of voxels (a pixel in 3 dimensions) from 2 different channels and a correlation of −1 indicates complete voxel disparity between the 2 channels being compared. Although RSV replicates solely in the cytosol, the close association of green RSV particles with DAPI signal (which stains both DNA and RNA) 40 min postentry afforded bleed-through colocalization during close proximity of RSV to the nucleus (Fig. 4c), reflected by a Pearson correlation that was greater than 0. The disparity of virus staining with DAPI at time zero, or when virus entry was inhibited by SB203580 (Fig. 4d), resulted in a Pearson correlation that was negative (green virus voxels and blue DAPI voxels do not overlap). The non-permeabilization control assay permitted staining of only extracellular virions; virus that trafficked to intracellular perinuclear regions was not stained, as reflected in the negative Pearson correlation of the "No PERM" control at 40 min postwarming in Fig. 4c.

We hypothesized that if p38 MAPK is activated upon contact with a virion, entry may be facilitated by the subsequent cellular activation and endocytosis that result from p38 MAPK activation. p38 MAPK can phosphorylate the Rab5 effectors EEA1 and Rabenosyn-5 on Thr-1392 and Ser-215, respectively (28), enhancing endocytic internalization. Therefore, this internalization enhancement activity of p38 MAPK may be utilized by viruses to increase virus entry efficiency.

Treatment of cells with p38 inhibitor SB203580 resulted in inhibition of ATF2 phosphorylation (Fig. 4b), as expected. Virus remained at the leading edge of the SB203580-treated cells at 40 min postinfection, in contrast to cells treated with DMSO vehicle; virus trafficked to more apical perinuclear regions in DMSO-treated cells, with virus moving entirely away from the basal surface. As in Fig. 4c, we quantified the localization of RSV particles to the perinuclear RNA staining by DAPI. Figure 4d shows a negative Pearson correlation at 40 min with SB203580 treatment (Pearson's correlation = −0.11 [$P \ll 0.001$]), whereas the Pearson correlation in the DMSO control is positive at this time point (Pearson's correlation = 0.03 [$P = 0.003$]).

The RSV nucleoprotein can be imaged 40 min postentry but not during p38 MAPK inhibition. To support the observations that RSV entry is dependent upon p38 MAP kinase activation, we stained cells under control and SB203580 treatment conditions using an anti-RSV-N antibody (Fig. 4e). The RSV-N protein (nucleocapsid) binds genomic and antigenomic viral RNAs to form an RNase-resistant nucleocapsid, packaged within virus virions. The RSV-N protein can be imaged 40 min postentry but not at 0 min postentry, suggesting that N protein imaging may be a measure of successful virion disassembly. Finally, SB203580 treatment resulted in a loss of RSV-N detection 40 min postentry, similar to the images at 0 min postentry (Fig. 4e), suggesting that SB203580 treatment inhibited release of RSV virion contents.

p38 MAPK inhibition by SB203580 slows influenza H1N1 virus traffic to the nucleus during virus entry. We also imaged the entry phase of influenza virus replication using H1N1/Weiss/43, in the presence and absence of p38 inhibitor SB203580. Influenza virus was detected using polyclonal goat anti-H1N1 influenza virus sera (see "Antibodies" in Materials and Methods). Influenza virus is one of the few RNA viruses that replicates in the nucleus, and it is dependent upon acidified late endosomes for fusion and delivery of virion contents within the target host cell, so that it utilizes different entry pathways than does RSV, which fuses at the cell surface and replicates in the cytosol. We costained influenza virus with early endosome antigen 1 (EEA1) since p38 MAPK has been shown to phosphorylate this protein and enhance endocytosis. We surmised that in the absence of p38 MAPK activation, in the presence of SB203580, influenza virus particles may be inhibited within EEA1-positive endosomes.

Figure 5a shows influenza virus particles sitting upon the surface of 1HAEo- bronchial epithelial cells prior to being warmed to 37°C. After 5 min of warming to 37°C, influenza virus ribonucleoproteins (rNPs) can be imaged within the nucleus of the control cells (Fig. 5b). There is apparently less

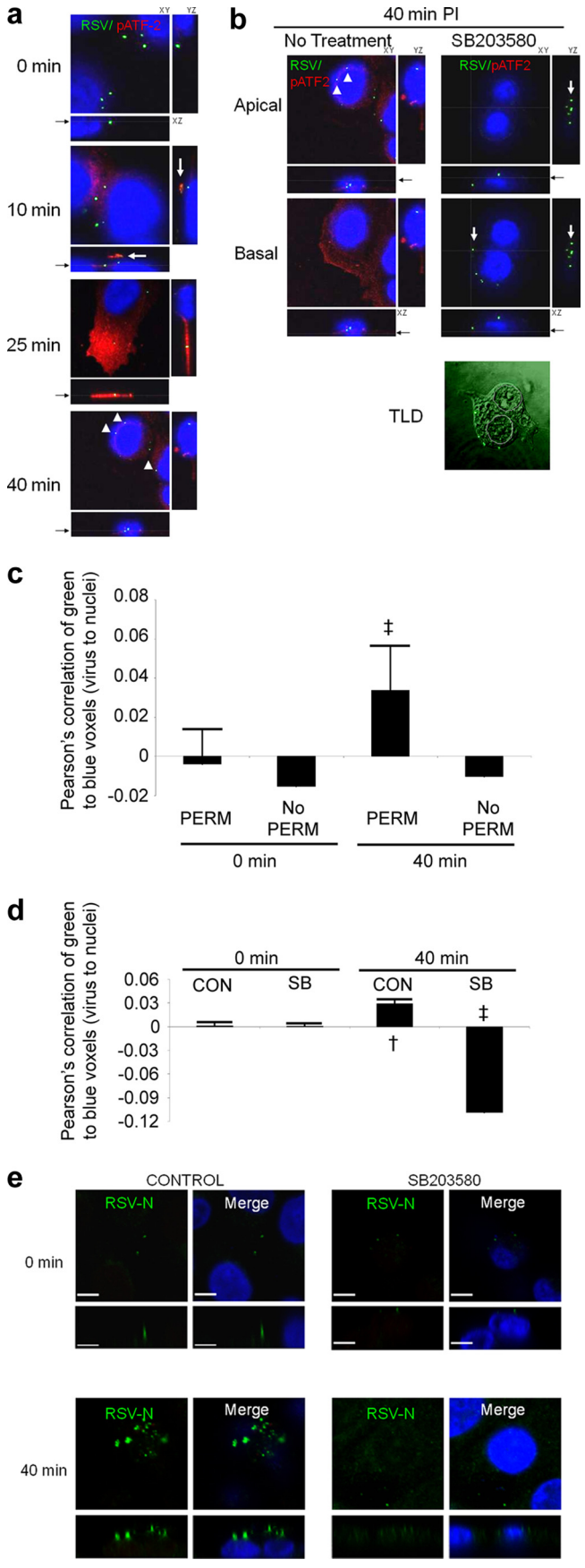

influenza virus protein in the nucleus of the SB203580-treated cells.

At 20 min after warming of SB203580-treated cells, we observed influenza virus particles within EEA1-positive endosomes, whereas all influenza virus protein appeared to have attained the nucleus of the control cells (Fig. 5c). Our results reflect those reported previously that p38 MAPK can enhance endocytosis internalization via EEA1 and Rabenosyn-5 (28), where we observed slowed trafficking of influenza virus to the nucleus upon inhibition of p38 MAPK activation. To quantitate the entry of influenza virus into the nucleus, we performed Pearson's colocalization analysis of nuclei stained with DAPI (blue voxels) and the green Alexa 488-stained influenza virus virions (green voxels), at the 0-, 5-, and 20-min time points of influenza virus entry into 1HAEo- cells. The values shown in Fig. 5d for the 20-min time point are greater than those of the Pearson correlation of RSV entry (Fig. 5e) since influenza virus, unlike RSV, enters and replicates within the nucleus. We noted that there was significantly less influenza virus detected within the nucleus at 5 and 20 min postinfection when p38 activation was inhibited with SB203580 (Fig. 5d), compared to the DMSO-treated control cells. Comparison of influenza virus and RSV entry was aided in part by the automatic counting of

FIG. 4. Viruses cause activation of ATF2 via p38 MAPK from the site of virus-host cell contact, during entry. (a) RSV-A2 was added to 1HAEo- cells on ice for 1 h at an MOI of 1, transferred to a 37°C incubator, fixed, and stained for RSV and phospho-ATF2 at the indicated time points after being warmed to 37°C. RSV is stained green, activated phospho-ATF2 (signaling product of activated p38 MAPK) is red, and nuclei are blue. The location of the presented XY slice is indicated with a gray line and a black arrow in the XZ pane. The 10-min image shows a burst of red (phospho-ATF2 [arrow]) above an internalized virus particle. The peak of phospho-ATF2 was most often seen at 25 min postinfection with a loss of signal at 40 min postinfection with residual signal remaining. Perinuclear localization of RSV was always observed by 40 min postinfection (arrowheads). (b) Activation of p38 MAPK was associated with apical perinuclear localization of virus after 40 min of entry with little or no basal localization of virion (arrowheads). Residual phospho-ATF2 activation is shown in red, RSV is shown in green, and nuclei were imaged blue with DAPI. Inhibitor (SB203580) suppression of p38 MAPK was associated with basal localization of virus at the leading edge of the cell/tissue culture margin (arrows), also illustrated by transmitted light detection (TLD) overlay. Note the less apparent red phospho-ATF2 staining (red; indicator of p38 MAPK activation) in the SB203580-treated cells in the right panels. The location of the presented XY slice is indicated with a gray line and a black arrow in the XZ aspect. (c) Pearson's correlation of image stacks (not shown) permeabilized (PERM) or not with 0.3% Triton X-100 during staining. ‡, $P < 0.001$. Permeabilization of cells during staining permits imaging of internalized virus particles/constituents. The Pearson correlation is positive 40 min after entry due to DAPI-RSV protein colocalization, which was lost if cells were not Triton X-100 permeabilized during staining. (d) Pearson's correlation of image stacks in panel a and accompanying SB203580 (SB)-treated controls (not shown) of green (Alexa 488) RSV particles to blue DAPI-stained nuclei. The graph shows a negative Pearson correlation at 40 min postwarming due to SB203580 inhibition of p38 MAPK, indicating that there was no RSV trafficking to perinuclear regions. †, $P < 0.005$; ‡, $P < 0.001$. CON, control. (e) RSV nucleoprotein (N) could be imaged during control conditions 40 min postentry, but it was lost with SB203580 treatment. Cells were infected, fixed, and stained as in panel a and stained for RSV-N using a monoclonal antibody (Materials and Methods). Bars, 6.2 μm. Results are representative of 4 independent experiments.

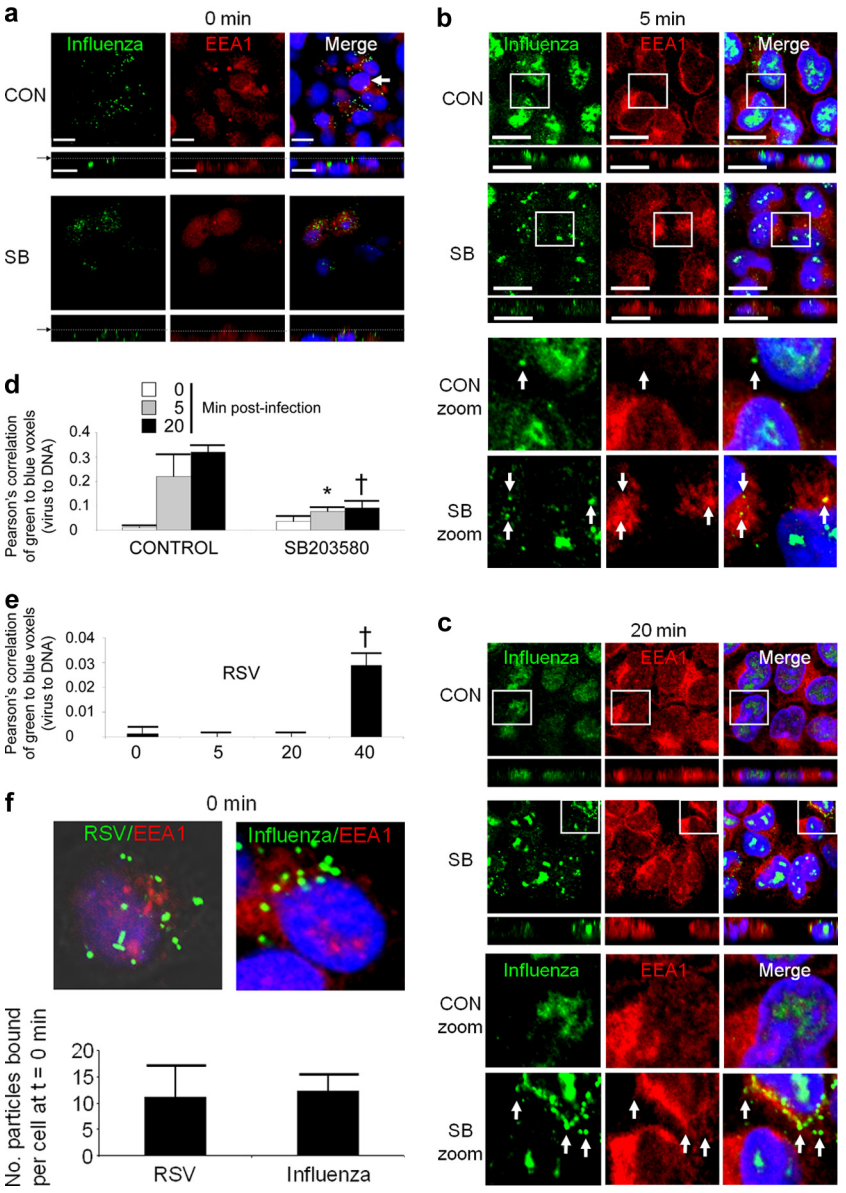

FIG. 5. Inhibition of p38 MAPK results in retention of influenza virus particles within early endosome antigen-positive endosomes. Images show confocal microscopy of influenza virus entry into upper airway 1HAEo- epithelial cells stained using an anti-H1N1 influenza virus goat polyclonal antibody. (a) Equivalent amounts of influenza virus (MOI, 3) were added to 1HAEo- cells treated with control (CON) DMSO and SB203580 (SB), on ice (0 min). The arrow indicates the XY image of a bisected nucleus, showing an absence of influenza virus localization to the nucleus at 0 min. Bars, 21 μm. (b) At 5 min postwarming most virus is visualized in the nucleus, whereas there is apparently less nuclear staining in the nucleus during treatment with SB203580. Bars, 10 μm. (c) At 20 min postwarming virus retention in EEA1-stained regions was most evident (arrows). (d) Pearson's correlation shows a significant loss of influenza virus localization to the nucleus during entry in the SB203580-treated cells compared to DMSO treatment control conditions (*, $P < 0.05$; †, $P < 0.005$). (e) Pearson's correlation of RSV during entry demonstrates the greater rate at which influenza virus attains the nucleus in panel d than at which RSV attains perinuclear regions by 40 min postwarming (†, $P < 0.005$). (f) Comparison of the number of influenza virus and RSV particles on cells, on ice, at 0 min postwarming, indicating that equivalent virus particle numbers were delivered to cells in entry comparison experiments. Results are representative of 4 independent experiments.

virus particles by Volocity software (Materials and Methods), which confirmed equivalent virus particle inputs (Fig. 5f).

Virus infection and subsequent TLR signaling can be neutralized with anti-TLR antibodies. Given the previous reports that the innate antiviral response may be activated by TLR4 binding to virus glycoproteins (15, 17, 21, 23, 38), we performed neutralization experiments with anti-TLR4 antibodies, followed by influenza virus and RSV inoculation. Since MyD88 is the adaptor molecule for several different TLRs (35), we wanted to test the possibility that p38-associated signaling could indeed be inhibited by blocking virus interaction with one of the TLRs. These experiments would assist us in determining whether a pathway(s) of MyD88-dependent pattern recognition may be responsible for rapid p38 MAPK activation during virus entry. We chose antibody neutralization since this technique is commonly used to block virus interactions with

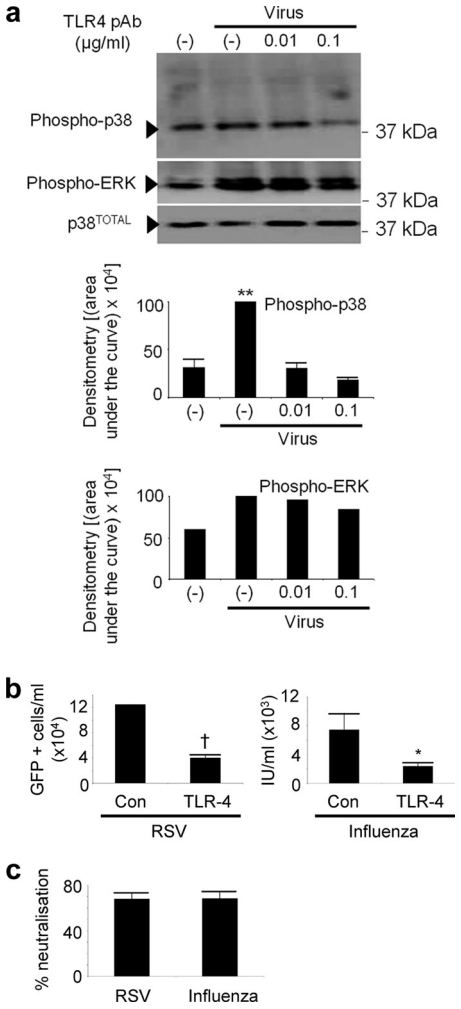

FIG. 6. Activation and phosphorylation of p38 MAPK/virus infection can be inhibited with anti-TLR4 antibodies. (a) An anti-TLR4 antibody titration was added to 1HAEo- cells for 30 min, RSV was added at an MOI of 1, cells were harvested with lysis buffer after 20 min of virus treatment, and phospho-p38 MAPK and phospho-ERK were detected, with total p38 as a loading control. pAb, polyclonal antibody. (b) Cells were treated as in panel a, but infection proceeded overnight before detection of RSV-GFP by flow cytometry and influenza virus infection via antibody staining and flow cytometry (Materials and Methods). The infection resulting from RSV-GFP was detected directly by flow cytometry of infected cells whereas influenza virus infection was detected by antibody staining of influenza virus-infected cells with a polyclonal anti-influenza virus antibody followed by staining with an Alexa 594 secondary antibody. (c) The percent neutralization assay was conducted on the 0.1-μg/ml anti-TLR4 dose for both RSV and influenza virus calculated from the data in panel b by dividing infection obtained in the presence of TLR4 antibody by control infection and multiplying the value by 100%. Results are representative of 2 independent experiments. Con, control.

receptors and to elucidate the physiology of virus-receptor interactions. Therefore, we postulated that if a TLR-virus interaction is genuine, then it (and all downstream effects) should, in principle, be neutralized with an anti-TLR4 receptor antibody. Figure 6a shows inhibition of p38 MAPK, but not ERK, signaling by treatment with an anti-TLR4 antibody at a concentration of 0.1 μg/ml. Figures 6b and c show that RSV and influenza virus infections were reduced similarly, 68% and 68.5%, respectively, by treatment with an anti-TLR4 antibody, compared to control antibody. Anti-TLR4 antibody added at higher concentrations caused enhanced p38 MAPK activation and corresponding increases in infection (data not shown). If TLR4 acted as an entry and fusion receptor for these viruses, we would have expected these higher concentrations of antibody to block infection in a dose-dependent manner (11, 13), rather than enhance infection as was observed.

p38 MAPK signaling is associated with clustering of TLR4 at the site of virus-cell attachment. Fluorescence confocal imaging of RSV, TLR4, and phospho-ATF2 demonstrated clustering of TLR4 at the site of RSV binding to the host cell, 10 min postinfection, whereas there was no TLR4 clustering or phospho-ATF2 signal observed in cells that were not bound by virus (Fig. 7a).

Overlapping confocal fluorescent signals that are attributed to colocalization/interaction of 2 or more different molecules can be the result of imaging artifacts due to fluorophore bleeding into the detection channel of the other fluorophore. We therefore wanted to determine the effect of blocking TLR4-virus interaction during entry in order to rule out potential imaging artifacts in the observation of the TLR4-virus clustering phenomenon. Custom bandwidth PMT filters of the Leica SP2 microscope were also utilized to eliminate colocalization artifacts (see Materials and Methods for technical descriptions). Goat polyclonal TLR4 antibody was added before virus addition and during virus entry. Low-magnification images in Fig. 7b show qualitative suppression of ATF2 phosphorylation due to 1 μg/ml of anti-TLR4 polyclonal antibody in a 25-min snapshot image.

Images in Fig. 7c, "0 min," show clusters of virus with TLR4 at 4°C (the ability of the receptor to remain mobile within the plane of the plasma membrane at 0°C has been described previously for influenza virus [1, 32]), under control conditions (Fig. 7c, arrows); there was also patching of TLR4 (green) beneath virus particles (cyan) under anti-TLR4 antibody treatment conditions (Fig. 7c, arrowheads). These results suggest that there is significant mobility of receptor at 4°C, supported by the work of others (1, 32). There were equivalent numbers of virus particles attached to the surface of infected cells under control and antibody treatment conditions, determined by automatic spot counting by Volocity software, suggesting that antibody treatment did not block virus interaction with the target cells (data not shown). The patching of TLR4 with virus occurred under antibody treatment conditions (Fig. 7d, inset), also suggesting that virus-TLR4 interaction was not affected by antibody treatment.

Treatment with antibody directed against TLR4 resulted in less coalescence of virus-TLR4 complex early after infection, as shown at the 0- (Fig. 7c), 10- (Fig. 7d), and 25-min (Fig. 7e) time points. Volocity software was used to identify virus-receptor complexes using a threshold of detection for virus cyan staining, and the complexes were then measured (Materials and Methods). Figure 7f shows the results of automatic Volocity measurements of virus-TLR4 complexes. Clusters of TLR4-virus complexes were significantly smaller at 0 min under antibody treatment conditions ($6.7 \times 10^{-1} \pm 2.4 \times 10^{-1}$ μm) than under control conditions ($1.2 \times 10^{0} \pm 4.8 \times 10^{-1}$ μm; $P = 0.004$). The size of virus-receptor complexes did not

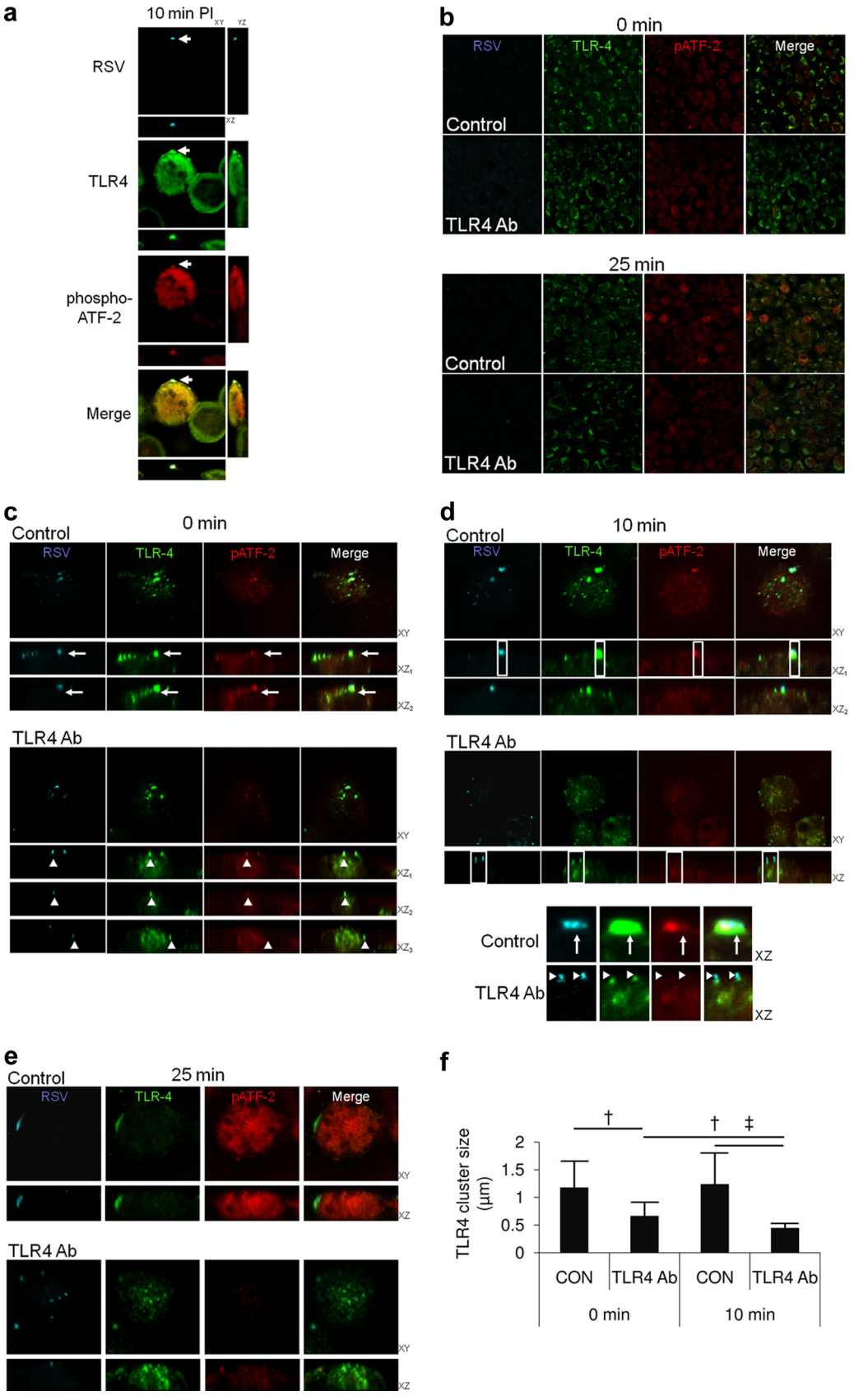
a
10 min PI
RSV
TLR4
phospho-ATF-2
Merge
b
0 min
RSV
TLR-4
pATF-2
Merge
Control
TLR4 Ab
25 min
Control
TLR4 Ab
c
0 min
Control
RSV
TLR-4
pATF-2
Merge
TLR4 Ab
d
10 min
Control
RSV
TLR-4
pATF-2
Merge
TLR4 Ab
Control
TLR4 Ab
e
25 min
Control
RSV
TLR-4
pATF-2
Merge
TLR4 Ab
f
TLR4 cluster size (μm)
2
1.5
1
0.5
0
CON
TLR4 Ab
CON
TLR4 Ab
0 min
10 min

change significantly between control 0- and 10-min postwarming time points; however, there was a significant decrease in virus-receptor cluster size in a comparison of the antibody treatment 0-min ($6.7 \times 10^{-1} \pm 2.4 \times 10^{-1}$ μm) and 10-min ($4.4 \times 10^{-1} \pm 8.0 \times 10^{-2}$ μm) time points ($P = 0.006$).

The XZ sections of the 10-min time point in the inset of Fig. 7d show an absence of RSV-TLR4 overlap in the TLR4 antibody-treated cell images, suggesting that TLR4 clustering at the site of virus attachment is not the product of image artifacts, though patching of TLR4 beneath virus particles continued to be evident in the presence of TLR4 antibody. Thus, these data support TLR4 binding and clustering around virus to activate p38 MAPK during virus entry.

DISCUSSION

We demonstrate that PRR recognition of virus, prior to host cell entry, is required to activate p38 MAPK via MyD88 to activate cellular internalization machinery. Our work also emphasizes that the virus entry receptor(s) is not the only protein with which virus interacts at the host cell surface prior to entry. The sugar residues that make up the virion surface provide an opportunity for the virus to induce signaling via nonreceptor host cell proteins, such as TLRs. Therefore, viruses have evolved mechanisms which they use to harness the activation of the innate immune system via pattern recognition receptors. We show that blocking TLR4 with an antibody prior to virus inoculation inhibited virus-induced p38 MAPK activation but also infection by both RSV and influenza virus. Influenza virus, which activated p38 MAPK to significantly greater levels than RSV, was internalized faster and more completely than RSV, of which some particles were not internalized. We believe that enveloped viruses like RSV and influenza virus trigger TLR4 activation upon initial interaction with the surface of the target host cell to drive virus internalization and entry. TLR4 has already been shown to recognize the surface glycoproteins from a diverse range of viruses (15, 23, 38). Furthermore, this glycosylation may be a necessity of virus entry, required by enveloped viruses to activate p38 MAPK.

The activation of p38 MAPK by virus interaction with PRRs is normally investigated in the context of the antiviral immune response. For instance, MyD88 deficiency in the host organism results in greater viral loads/viremia (4, 7, 41, 50), due to a lack of antiviral CD8 T-cell expansion (36). Here we show that viruses have evolved the ability to activate their entry and replication in parallel with these responses, in nonimmune cells. This strategy has been successful such that p38 MAPK activation has evolved as a critical tropism determinant of virus replication, rescued in MyD88 KO cells by ectopic activation of p38. An effective approach of treating viral replication may be, paradoxically, to inhibit the host antiviral response mediated via p38 MAPK activation, as we have demonstrated *in vivo* (29). MyD88 KO cells endocytose less actively than do their WT counterparts, and this lack of activity may be a reason why these cells are less infectable (25), since influenza virus, for example, is well known to be dependent upon endocytosis for successful host cell entry.

Our results are consistent with the kinetics of influenza virus entry reported previously (2). In comparison, we noted that RSV entry requires significantly more time to attain regions within the cell that are conducive to virus replication than influenza virus. Influenza virus also activated p38 MAPK to levels that were about 10-fold greater than those of RSV, so influenza virus may have evolved to activate this signaling molecule to higher levels to enhance endocytic uptake and entry. The report that p38 MAPK enhances endocytosis via Rabenosyn-5 and EEA1 is consistent with what we observed for influenza virus entry, where we observed significant localization of influenza virus with the early endosome network during treatment with a p38 inhibitor. However, p38 inhibition did not completely halt influenza virus entry, as it did with RSV entry, suggesting that other minor signaling pathways may be activated by influenza virus as well that could drive entry at a lower rate. But we do not think that alternate signaling pathways are associated with the alternate nonclathrin route of entry described for influenza virus (24, 31, 43), since this alternate pathway internalizes, on average, 40% of virus (2), and we observed a 10-fold loss of influenza virus correlation with nuclear staining when p38 MAPK was inhibited.

p38 was not always activated at early time points postinfection, as was the case for CVB3. It has been shown previously that p38 MAPK activation during later replication time points of CVB3 activates caspase-3 initiation of cell death, a require-

FIG. 7. TLR4 clustering around virus particles is associated with p38 MAPK activation during virus entry. (a and b) Phospho-ATF2, TLR4, and RSV were imaged during virus entry into 1HAEo- cells using a Leica SP2 confocal microscope. Virus was added to cells on ice for 1 h at an MOI of 1, washed and transferred to a 37°C incubator for the indicated time points, and fixed and stained for RSV, TLR4, and phospho-ATF2 as an indicator of p38 MAPK activation. (a) Phospho-ATF2 staining was associated with TLR4 clustering at the point of virus attachment to the host cell 10 min postinfection (PI) (arrow). Shown are 2 cells: one is bound by virus (arrow) and the other is not (note lack of TLR4 clustering and red phospho-ATF2 staining). Clustering of TLR4 and phospho-ATF2 staining were absent from cells not bound by virus (adjacent cell). (b) Cells were imaged as in panel a, but an anti-TLR4 polyclonal antibody (1 μg/ml) was added to the cells 1 h before and during incubation with virus inoculum or with control isotype antibody as a control. Low-magnification images show that anti-TLR4 antibody treatment results in less phospho-ATF-2 activation 25 min after warming to 37°C. (c to e) Higher-magnification image scans of the cells in panel b show reduced clustering of virus with TLR4 at 0 (c), 10 (d), and 25 (e) min after being warmed to 37°C due to anti-TLR4 antibody treatment. (d, inset) The XZ sections were enlarged from the 10-min postentry time point to show reduced TLR4 clustering under anti-TLR4 antibody treatment conditions. Enlarged XZ sections also demonstrate specificity of virus and TLR4 staining/imaging; TLR4 clustering is not an imaging artifact due to fluorescent dye bleed-through, since distinct virus particles can be seen atop TLR4 clusters under the anti-TLR4 antibody treatment conditions (arrowheads). Phospho-ATF2 staining did not follow the pixel density of the TLR4 channel, suggesting that this signal was not a result of green Alexa 488 (TLR4) channel into the red Alexa 594 channel (phospho-ATF2 [arrow]). Large TLR4-to-RSV clustering events at 25 min postwarming were associated with strong phospho-ATF2 staining and were absent in culture wells treated with anti-TLR4 antibody (1 μg/ml). (f) Volocity software identified TLR4 clustering that was positive for RSV staining, which was measured automatically in μm throughout the image Z-stacks (Materials and Methods; †, $P < 0.005$; ‡, $P < 0.001$). Results are representative of 3 independent experiments. CON, control.

ment of efficient progeny virus release (42). Si et al. also showed that CVB3 activated p38 very weakly or not at all during entry, consistent with our current results. In the absence of p38 MAPK activation during virus entry, we have shown that picornaviruses may utilize ERK-induced endocytosis, which is activated by virus entry receptor binding (30); transmembrane protein entry receptor interaction with subsequent MAPK signaling may be required by these viruses to activate cellular internalization mechanisms. Adenovirus was also relatively unable to activate the MAPKs during entry. Taken together, our results suggest that the absence of an envelope or the lack of glycosylation on these viruses may preclude them from PRR activation during entry and that p38 can be activated by other mechanisms at later replication time points. Moreover, among the enveloped viruses we detected significantly more MAPK activation by influenza virus than by any other virus studied, perhaps contributing to the virulence of this pathogen.

We noted that ERK MAPK was activated in MyD88 KO cells whereas p38 MAPK activation was absent. These two MAPKs are often referred to interchangeably; however, we have shown here that these 2 kinases had very different activation requirements with regard to MyD88 in fibroblasts and epithelial cells. We have shown that ERK activation is required for virus entry and infection, but alone, it was clearly not sufficient for the productive infection of pulmonary fibroblasts, since p38 MAPK must also be activated to effect entry and infection. However, epithelial cells and fibroblasts are not the only cells infected within the airways; alveolar macrophages and other immune cells are often the first cell types to be infected by respiratory viruses. Whether viruses require the same p38 and ERK MAPK signaling for infection of immune cells remains to be seen and is a potential research focus, particularly since these cells tend to express a different repertoire of pattern recognition receptors.

Latz et al. showed that TLR4-mediated internalization of LPS is independent of NF-κB activation (25), which is consistent with our findings. We propose that the receptor used by a virus to activate cellular MAPKs to permit expedient uptake be termed the signaling receptor, in conjunction with the protein or carbohydrate entry-fusion receptor required for host cell targeting and virus-cell fusion. The PRRs are other receptors that the virus may bind to enhance entry, in conjunction with the entry-fusion receptor; the entry and signaling receptors may comprise an entry complex that is unique to each virus.

We have shown that the p38 MAPK inhibitor SB203580 is well tolerated and effective at inhibiting viral replication *in vivo*, as we have shown previously (29). We now believe that p38 inhibitors are potential broad-spectrum antiviral drugs that could be administered to a patient with suspected viral infection prior to laboratory virus identification. This strategy could also be useful as a temporizing measure during viral outbreaks in order to inhibit viral replication prior to identification of the specific viral pathogen.

ACKNOWLEDGMENTS

This work was supported by grants from the Canadian Institutes of Health Research (CIHR). D.M. and T.L.H. are supported by Impact-STIHR fellowships. D.M. is supported by the Heart and Stroke Foundation of Canada and the Myocarditis Foundation.

REFERENCES

1. **Anderson, C. M., G. N. Georgiou, I. E. Morrison, G. V. Stevenson, and R. J. Cherry.** 1992. Tracking of cell surface receptors by fluorescence digital imaging microscopy using a charge-coupled device camera. Low-density lipoprotein and influenza virus receptor mobility at 4 degrees C. J. Cell Sci. **101:**415–425.
2. **Bachi, T., W. Gerhard, and J. W. Yewdell.** 1985. Monoclonal antibodies detect different forms of influenza virus hemagglutinin during viral penetration and biosynthesis. J. Virol. **55:**307–313.
3. **Beigel, J. H., J. Farrar, A. M. Han, F. G. Hayden, R. Hyer, M. D. de Jong, S. Lochindarat, T. K. Nguyen, T. H. Nguyen, T. H. Tran, A. Nicoll, S. Touch, and K. Y. Yuen.** 2005. Avian influenza A (H5N1) infection in humans. N. Engl. J. Med. **353:**1374–1385.
4. **Browne, E. P., and D. R. Littman.** 2009. Myd88 is required for an antibody response to retroviral infection. PLoS Pathog. **5:**e1000298.
5. **Cano, E., C. A. Hazzalin, and L. C. Mahadevan.** 1994. Anisomycin-activated protein kinases p45 and p55 but not mitogen-activated protein kinases ERK-1 and -2 are implicated in the induction of c-fos and c-jun. Mol. Cell. Biol. **14:**7352–7362.
6. **Dorscheid, D. R., A. E. Conforti, K. J. Hamann, K. F. Rabe, and S. R. White.** 1999. Characterization of cell surface lectin-binding patterns of human airway epithelium. Histochem. J. **31:**145–151.
7. **Dyer, K. D., C. M. Percopo, E. R. Fischer, S. J. Gabryszewski, and H. F. Rosenberg.** 2009. Pneumoviruses infect eosinophils and elicit MyD88-dependent release of chemoattractant cytokines and interleukin-6. Blood **114:**2649–2656.
8. **Esfandiarei, M., S. Boroomand, A. Suarez, X. Si, M. Rahmani, and B. McManus.** 2007. Coxsackievirus B3 activates nuclear factor kappa B transcription factor via a phosphatidylinositol-3 kinase/protein kinase B-dependent pathway to improve host cell viability. Cell. Microbiol. **9:**2358–2371.
9. **Esfandiarei, M., H. Luo, B. Yanagawa, A. Suarez, D. Dabiri, J. Zhang, and B. M. McManus.** 2004. Protein kinase B/Akt regulates coxsackievirus B3 replication through a mechanism which is not caspase dependent. J. Virol. **78:**4289–4298.
10. **Esfandiarei, M., A. Suarez, A. Amaral, X. Si, M. Rahmani, S. Dedhar, and B. M. McManus.** 2006. Novel role for integrin-linked kinase in modulation of coxsackievirus B3 replication and virus-induced cardiomyocyte injury. Circ. Res. **99:**354–361.
11. **Evans, D.** 2008. Viral receptors, p. 319–324. *In* B. W. J. Mahy and M. H. V. van Regenmortel (ed.), Encyclopedia of virology, 3rd ed. Academic Press, New York, NY.
12. **Feuer, R., I. Mena, R. Pagarigan, M. K. Slifka, and J. L. Whitton.** 2002. Cell cycle status affects coxsackievirus replication, persistence, and reactivation in vitro. J. Virol. **76:**4430–4440.
13. **Flint, S. J., et al.** 2000. Principles of virology: molecular biology, pathogenesis, and control. ASM Press, Washington, DC.
14. **Gambotto, A., S. M. Barratt-Boyes, M. D. de Jong, G. Neumann, and Y. Kawaoka.** 2008. Human infection with highly pathogenic H5N1 influenza virus. Lancet **371:**1464–1475.
15. **Hahm, B., J. H. Cho, and M. B. Oldstone.** 2007. Measles virus-dendritic cell interaction via SLAM inhibits innate immunity: selective signaling through TLR4 but not other TLRs mediates suppression of IL-12 synthesis. Virology **358:**251–257.
16. **Hall, C. B., G. A. Weinberg, M. K. Iwane, A. K. Blumkin, K. M. Edwards, M. A. Staat, P. Auinger, M. R. Griffin, K. A. Poehling, D. Erdman, C. G. Grijalva, Y. Zhu, and P. Szilagyi.** 2009. The burden of respiratory syncytial virus infection in young children. N. Engl. J. Med. **360:**588–598.
17. **Hartshorn, K. L., K. Sastry, M. R. White, E. M. Anders, M. Super, R. A. Ezekowitz, and A. I. Tauber.** 1993. Human mannose-binding protein functions as an opsonin for influenza A viruses. J. Clin. Invest. **91:**1414–1420.
18. **Hazzalin, C. A., E. Cano, A. Cuenda, M. J. Barratt, P. Cohen, and L. C. Mahadevan.** 1996. p38/RK is essential for stress-induced nuclear responses: JNK/SAPKs and c-Jun/ATF-2 phosphorylation are insufficient. Curr. Biol. **6:**1028–1031.
19. **Holloway, G., and B. S. Coulson.** 2006. Rotavirus activates JNK and p38 signaling pathways in intestinal cells, leading to AP-1-driven transcriptional responses and enhanced virus replication. J. Virol. **80:**10624–10633.
20. **Jafri, M., B. Donnelly, M. McNeal, R. Ward, and G. Tiao.** 2007. MAPK signaling contributes to rotaviral-induced cholangiocyte injury and viral replication. Surgery **142:**192–201.
21. **Ji, X., G. G. Olinger, S. Aris, Y. Chen, H. Gewurz, and G. T. Spear.** 2005. Mannose-binding lectin binds to Ebola and Marburg envelope glycoproteins, resulting in blocking of virus interaction with DC-SIGN and complement-mediated virus neutralization. J. Gen. Virol. **86:**2535–2542.
22. **Kopp, E., and R. Medzhitov.** 2003. Recognition of microbial infection by Toll-like receptors. Curr. Opin. Immunol. **15:**396–401.
23. **Kurt-Jones, E. A., L. Popova, L. Kwinn, L. M. Haynes, L. P. Jones, R. A. Tripp, E. E. Walsh, M. W. Freeman, D. T. Golenbock, L. J. Anderson, and R. W. Finberg.** 2000. Pattern recognition receptors TLR4 and CD14 mediate response to respiratory syncytial virus. Nat. Immunol. **1:**398–401.

24. **Lakadamyali, M., M. J. Rust, and X. Zhuang.** 2004. Endocytosis of influenza viruses. Microbes Infect. **6:**929–936.
25. **Latz, E., A. Visintin, E. Lien, K. A. Fitzgerald, B. G. Monks, E. A. Kurt-Jones, D. T. Golenbock, and T. Espevik.** 2002. Lipopolysaccharide rapidly traffics to and from the Golgi apparatus with the toll-like receptor 4-MD-2-CD14 complex in a process that is distinct from the initiation of signal transduction. J. Biol. Chem. **277:**47834–47843.
26. **Luo, H., B. Yanagawa, J. Zhang, Z. Luo, M. Zhang, M. Esfandiarei, C. Carthy, J. E. Wilson, D. Yang, and B. M. McManus.** 2002. Coxsackievirus B3 replication is reduced by inhibition of the extracellular signal-regulated kinase (ERK) signaling pathway. J. Virol. **76:**3365–3373.
27. **Luo, H., J. Zhang, C. Cheung, A. Suarez, B. M. McManus, and D. Yang.** 2003. Proteasome inhibition reduces coxsackievirus B3 replication in murine cardiomyocytes. Am. J. Pathol. **163:**381–385.
28. **Mace, G., M. Miaczynska, M. Zerial, and A. R. Nebreda.** 2005. Phosphorylation of EEA1 by p38 MAP kinase regulates mu opioid receptor endocytosis. EMBO J. **24:**3235–3246.
29. **Marchant, D., Y. Dou, H. Luo, F. S. Garmaroudi, J. E. McDonough, X. Si, E. Walker, Z. Luo, A. Arner, R. G. Hegele, I. Laher, and B. M. McManus.** 2009. Bosentan enhances viral load via endothelin-1 receptor type-A-mediated p38 mitogen-activated protein kinase activation while improving cardiac function during coxsackievirus-induced myocarditis. Circ. Res. **104:**813–821.
30. **Marchant, D., A. Sall, X. Si, T. Abraham, W. Wu, Z. Luo, T. Petersen, R. G. Hegele, and B. M. McManus.** 2009. ERK MAP kinase-activated Arf6 trafficking directs coxsackievirus type B3 into an unproductive compartment during virus host-cell entry. J. Gen. Virol. **90:**854–862.
31. **Matlin, K. S., H. Reggio, A. Helenius, and K. Simons.** 1981. Infectious entry pathway of influenza virus in a canine kidney cell line. J. Cell Biol. **91:**601–613.
32. **Morrison, I. E., C. M. Anderson, G. N. Georgiou, G. V. Stevenson, and R. J. Cherry.** 1994. Analysis of receptor clustering on cell surfaces by imaging fluorescent particles. Biophys. J. **67:**1280–1290.
33. **Moscona, A.** 2009. Global transmission of oseltamivir-resistant influenza. N. Engl. J. Med. **360:**953–956.
34. **Ogawa, T., T. Hayashi, S. Kyoizumi, Y. Kusunoki, K. Nakachi, D. G. MacPhee, J. E. Trosko, K. Kataoka, and N. Yorioka.** 2004. Anisomycin downregulates gap-junctional intercellular communication via the p38 MAP-kinase pathway. J. Cell Sci. **117:**2087–2096.
35. **O'Neill, L. A.** 2002. Signal transduction pathways activated by the IL-1 receptor/toll-like receptor superfamily. Curr. Top. Microbiol. Immunol. **270:** 47–61.
36. **Rahman, A. H., W. Cui, D. F. Larosa, D. K. Taylor, J. Zhang, D. R. Goldstein, E. J. Wherry, S. M. Kaech, and L. A. Turka.** 2008. MyD88 plays a critical T cell-intrinsic role in supporting CD8 T cell expansion during acute lymphocytic choriomeningitis virus infection. J. Immunol. **181:**3804–3810.
37. **Rahmani, M., J. T. Read, J. M. Carthy, P. C. McDonald, B. W. Wong, M. Esfandiarei, X. Si, Z. Luo, H. Luo, P. S. Rennie, and B. M. McManus.** 2005. Regulation of the versican promoter by the beta-catenin-T-cell factor complex in vascular smooth muscle cells. J. Biol. Chem. **280:**13019–13028.
38. **Rolland, A., E. Jouvin-Marche, C. Viret, M. Faure, H. Perron, and P. N. Marche.** 2006. The envelope protein of a human endogenous retrovirus-W family activates innate immunity through CD14/TLR4 and promotes Th1-like responses. J. Immunol. **176:**7636–7644.
39. **Romero, J. R.** 2008. Pediatric group B coxsackievirus infections. Curr. Top. Microbiol. Immunol. **323:**223–239.
40. **Rota, P. A., M. S. Oberste, S. S. Monroe, W. A. Nix, R. Campagnoli, J. P. Icenogle, S. Penaranda, B. Bankamp, K. Maher, M. H. Chen, S. Tong, A. Tamin, L. Lowe, M. Frace, J. L. DeRisi, Q. Chen, D. Wang, D. D. Erdman, T. C. Peret, C. Burns, T. G. Ksiazek, P. E. Rollin, A. Sanchez, S. Liffick, B. Holloway, J. Limor, K. McCaustland, M. Olsen-Rasmussen, R. Fouchier, S. Gunther, A. D. Osterhaus, C. Drosten, M. A. Pallansch, L. J. Anderson, and W. J. Bellini.** 2003. Characterization of a novel coronavirus associated with severe acute respiratory syndrome. Science **300:**1394–1399.
41. **Sheahan, T., T. E. Morrison, W. Funkhouser, S. Uematsu, S. Akira, R. S. Baric, and M. T. Heise.** 2008. MyD88 is required for protection from lethal infection with a mouse-adapted SARS-CoV. PLoS Pathog. **4:**e1000240.
42. **Si, X., H. Luo, A. Morgan, J. Zhang, J. Wong, J. Yuan, M. Esfandiarei, G. Gao, C. Cheung, and B. M. McManus.** 2005. Stress-activated protein kinases are involved in coxsackievirus B3 viral progeny release. J. Virol. **79:**13875–13881.
43. **Sieczkarski, S. B., and G. R. Whittaker.** 2002. Influenza virus can enter and infect cells in the absence of clathrin-mediated endocytosis. J. Virol. **76:** 10455–10464.
44. **Slifka, M. K., R. Pagarigan, I. Mena, R. Feuer, and J. L. Whitton.** 2001. Using recombinant coxsackievirus B3 to evaluate the induction and protective efficacy of CD8+ T cells during picornavirus infection. J. Virol. **75:**2377–2387.
45. **Tao, T., A. P. Durbin, S. S. Whitehead, F. Davoodi, P. L. Collins, and B. R. Murphy.** 1998. Recovery of a fully viable chimeric human parainfluenza virus (PIV) type 3 in which the hemagglutinin-neuraminidase and fusion glycoproteins have been replaced by those of PIV type 1. J. Virol. **72:**2955–2961.
46. **Techaarpornkul, S., P. L. Collins, and M. E. Peeples.** 2002. Respiratory syncytial virus with the fusion protein as its only viral glycoprotein is less dependent on cellular glycosaminoglycans for attachment than complete virus. Virology **294:**296–304.
47. **Yuan, J., J. Zhang, B. W. Wong, X. Si, J. Wong, D. Yang, and H. Luo.** 2005. Inhibition of glycogen synthase kinase 3beta suppresses coxsackievirus-induced cytopathic effect and apoptosis via stabilization of beta-catenin. Cell Death Differ. **12:**1097–1106.
48. **Zhang, L., A. Bukreyev, C. I. Thompson, B. Watson, M. E. Peeples, P. L. Collins, and R. J. Pickles.** 2005. Infection of ciliated cells by human parainfluenza virus type 3 in an in vitro model of human airway epithelium. J. Virol. **79:**1113–1124.
49. **Zhang, L., M. E. Peeples, R. C. Boucher, P. L. Collins, and R. J. Pickles.** 2002. Respiratory syncytial virus infection of human airway epithelial cells is polarized, specific to ciliated cells, and without obvious cytopathology. J. Virol. **76:**5654–5666.
50. **Zhu, J., X. Huang, and Y. Yang.** 2009. The TLR9-MyD88 pathway is critical for adaptive immune responses to adeno-associated virus gene therapy vectors in mice. J. Clin. Invest. **119:**2388–2398.